The fluctuation-dissipation relation holds for a macroscopic tracer in an active bath

Dima Boriskovsky,[1] Benjamin Lindner,[2,3] and Yael Roichman[1,4,*]

[1] *Raymond & Beverly Sackler School of Physics and Astronomy, Tel Aviv University, Tel Aviv 6997801, Israel*
[2] *Bernstein Center for Computational Neuroscience Berlin, Philippstr. 13, Haus 2, 10115 Berlin, Germany*
[3] *Physics Department of Humboldt University Berlin, Newtonstr. 15, 12489 Berlin, Germany*
[4] *Raymond & Beverly Sackler School of Chemistry, Tel Aviv University, Tel Aviv 6997801, Israel*

SUPPLEMENTARY INFORMATION

The bbot bath characteristics

We characterize the properties of the bbot *active gas* in the harmonic trap, and its effect on the motion of a passive tracer. A single bbot in a parabolic arena adopts a circular path when it has sufficient inertia [1]. Additionally, the bbot favors clockwise rotation reflecting its inherent chirality, which stems from an asymmetric motor.

By introducing additional bbots into the harmonic trap, collisions between them randomize their motion. This effect increases with the bbot number N_b (see Fig. 1**A** and **B**). We observe that the speed and velocity distributions remain independent of N_b, with a mean speed $\langle v_b \rangle \approx 11$cm/s (see Fig. 1**C** and **D**). We also find that the bbots are heavy enough to ensure no air-stream effect on their motion during a response measurement (see Fig. 2).

In Fig. 3**A**, **B** we compare typical trajectories of a bbot and a tracer under the same setup. Note that the tracer's motion is randomized even for $N_b = 3$, where collisions are rare. We evaluate the net chirality of the bbot bath by counting the clockwise $(+1)$ and anticlockwise (-1) crossings of a central line at $x = 0$. By tracking 200 bbot trajectories ($t \in [0, 5]$s), we obtain the sum of bbot rotations $\pm n$ per frame, and a probability distribution $P(n)$ (see Fig. 3**C**). We find that the systems attain a net clockwise chirality that is reduced by increasing N_b. In comparison, we provide the chirality of the tracer particle's motion. The latter results in small values and vanishes for high N_b (Fig. 3**D**).

A passive tracer in a bbot bath

The tracer performs a Brownian-like motion, with a Boltzmann-like PDF for $N_b = 15$ (Fig. 4). The main effect of the bath density on the tracer is an increase in the number of collisions and the energy transferred to it. Thus, once the collision frequency is sufficient, the PDF reflects the gravitational potential of the bowl.

We note that a bbot can both tumble (fall on its side) and get back up, due to random collisions with other bbots. Once N_b becomes sufficiently large, tumbled bbots form long-lived static clusters at the center trap region (see an example in Fig. 5**A**). A similar phenomenon is observed in parabolic arenas with different sizes and curvatures. The latter can prevent the tracer from accessing the center trap region. In turn, for $N_b = 17$, we observe a flat region in the center of the tracer's position distribution (Fig. 5**B**). Nevertheless, the FDR holds in this case. Due to this technical issue, we cannot conduct a meaningful FDR test above $N_b > 17$ and, therefore, cannot exclude FDR violations for higher densities. Alternatively, we observe that the FDR holds by changing the bbot speed but keeping N_b constant. Namely, the FDR is valid with $T_{\text{eff}} \sim \langle \Delta x \rangle_0$ for $N_b = 6$ *fast bbots* (see Fig. 6), suggesting the validity of the FDR for varying bath particle activities.

We furthermore add the following supplemental results: A FDR test with constant N_b and increasing perturbation amplitudes (Fig. 7); The passive response of the tracer to a step-perturbation in the absence of bbots (Fig. 8); The tracer's restitution coefficient measurement (Fig. 9); T_{eff} versus the kinetic temperature $T_v \sim \langle v^2 \rangle$ (Fig. 10); Individual FDR results for all N_b (Fig. 11).

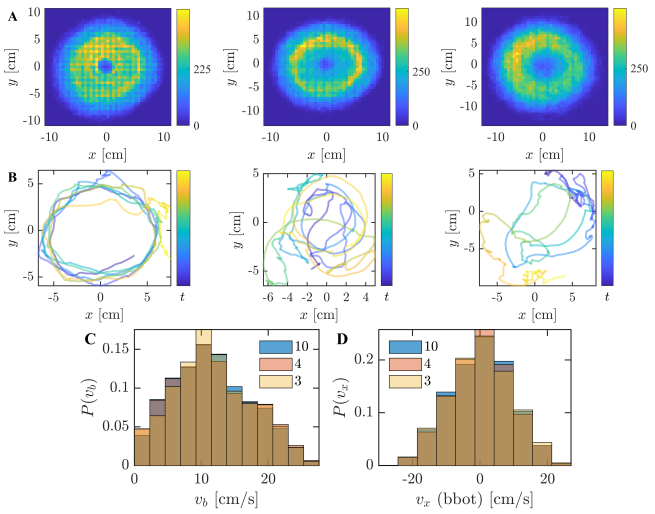

FIG. 1. **Distributions and typical trajectories of bbots for different densities. A.** The total ensemble positional distribution of the bbots in the harmonic trap. The results are for $N_b = 3$, 4, and 10, from left to right respectively, obtained by tracking all of the bbots for 30 minutes. **B.** Typical single bbot trajectories, $t \in [0, 15]s$. The bbot speed (**C.**) and velocity (**D.**) distributions remain independent of N_b.

* roichman@tauex.tau.ac.il

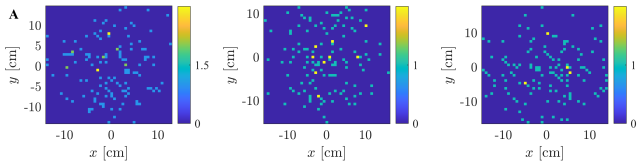

FIG. 2. **The external air-stream does not affect the bbots.** We show the difference of the spatial bbot distributions with the fan on and off, for $N_b = 3$, 4, and 10, from left to right, respectively, showing that the bbots are not affected by the fan's air-flow.

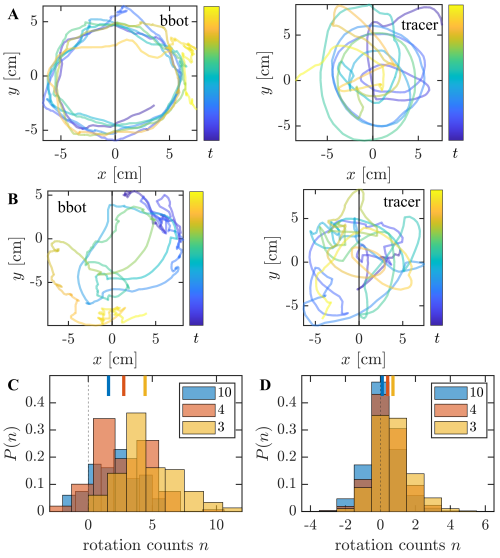

FIG. 3. **The system's chirality.** Typical single bbot and tracer trajectories, in a system with $N_b = 3$ (**A**) and $N_b = 10$ (**B**). **C.** The distribution of bbot instantaneous rotations $\pm n$ across a central line at $x = 0$, where $n > 0$ indicates favored clockwise direction. Obtained by tracking 200 bbots trajectories ($t \in [0, 5]s$). The upper lines are the means of $P(n)$, showing that net chirality is reduced by increasing N_b. **D.** The same chirality analysis for the passive tracer.

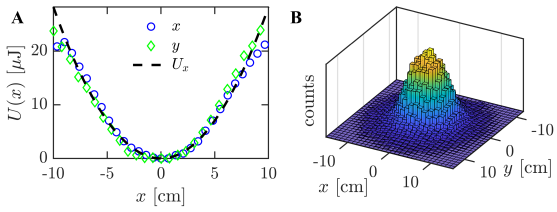

FIG. 4. **Spatial probability distribution and effective potential. A.** The physical trapping potential $U_x(x) = mgax^2$ (dashed line), compared to the Boltzmann statistics based experimental estimate of the potential. The results are obtained by averaging $M = 375$ tracer position time-sequences, with $t \in [0, 30]$ s, in a $N_b = 15$ bbot bath. **B.** A 3D (x, y) tracer position histogram.

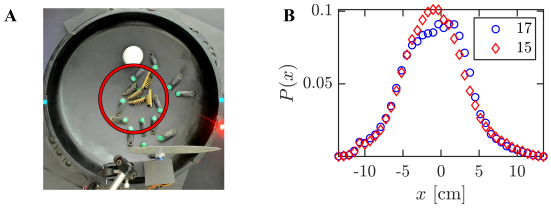

FIG. 5. **A.** Snapshot of an experiment with $N_b = 17$, showing a temporal static cluster of tumbled bbots in the center trap region. **B.** The tracer's position probability distribution for $N_b = 17$, showing a flat region in the center, reflecting the physical exclusion by static bbot clusters.

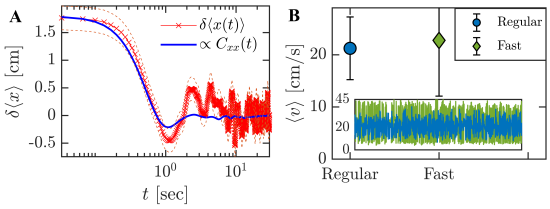

FIG. 6. **FDR test with faster bbots. A.** Generalized FDR test with $k_B T_{\text{eff}} = k\langle x^2\rangle_0$ for $N_b = 6$ fast bbots, 9 V fan operating voltage (weak perturbation), and an average over $M = 375$ perturbation sequences. **B.** Average individual speed of a single bbot walking in a parabolic arena. Regular bbot (circle), as used in our work, and a fast bbot (diamond), as used in panel (A). The inset displays typical sequences of instantaneous speeds $v(t)$ in cm/s for regular (blue) and fast (green) bbots.

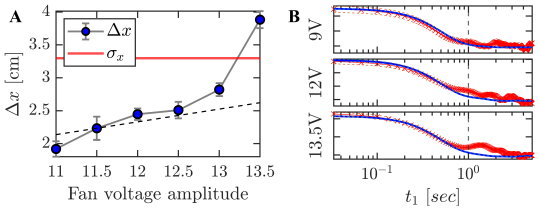

FIG. 7. **The generalized FDR under different perturbation amplitudes. A.** The mean displacement Δx under a perturbation of a tracer in a $N_b = 10$ bbot bath, as a function of fan operating voltage V (error bars are standard errors). The applied force $F_0 = k\Delta x$ increases above $V = 11$V. The tracer's position standard deviation, σ_x, is used to define the range of small perturbations (solid line). The dashed line is a linear fit of the first 4 data points, with $\Delta x = 0.19 \cdot V$, whereas $V = 13$V and 13.5V are out of the linear regime. **B.** The generalized FDRs with $T_{\text{eff}} \sim \langle \Delta x^2\rangle_0$ are plotted for $V = 9$, 12, 13.5 V, with $N_b = 10$. The results present an average over $M = 375$ perturbation sequences.

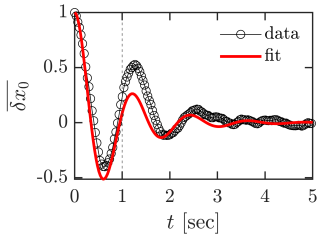

FIG. 8. **Passive response measurement.** We probe the tracer's coupling to the trap in the absence of collisions by measuring the (deterministic) response δx_0 to a step-perturbation with the bbots removed (13.5V fan voltage, abruptly switched off at $t = 0$). Considering the tracer relaxes as a damped harmonic oscillator with natural frequency $(\tau_\Omega^0)^{-1} = \sqrt{k/m} = 5.3\ \mathrm{s}^{-1}$, the passive damping timescale is obtained by fitting the normalized response to Eq. 2, $\tau_r^0 = 0.9$s.

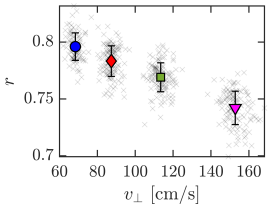

FIG. 9. **Tracer's coefficient of restitution versus impact velocities.** The restitution coefficient r was determined from the sound signal emitted by the styrofoam ball (the tracer) bouncing repeatedly off a surface, as detailed in Ref. [2]. We obtain r by measuring the time lag between consecutive impacts: $r_i = |v_i'/v_i| = (t_{i+1} - t_i)/(t_i - t_{i-1})$, for an impact velocity $v_i = \frac{g}{2}(t_{i-1} - t_i)$, $i = 2, 3, ...$ Here, v_i and v_i' are the normal pre- and post-collision velocities occurring at time t_i, and $g = 9.81\mathrm{m/s}^2$ is the gravitational acceleration. The plot shows four successive impacts of a repeated experiment (50 trials), with mean values from last to first respectively: $r = 0.79$ (circle), 0.78 (diamond), 0.76 (square), 0.74 (triangle), for $v_\perp = 68.37$, 87.35, 113.4, 152.83 cm/s.

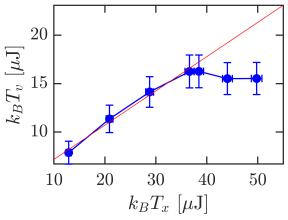

FIG. 10. **Kinetic and potential temperatures.** The potential temperature, $k_B T_x = k\langle \Delta x^2 \rangle_0$, is plotted versus the kinetic temperature of the tracer, $k_B T_v = m\langle v^2 \rangle_0$. We find a linear relation for the range of $3 \geq N_b \leq 10$. The red line is the best linear fit for this range.

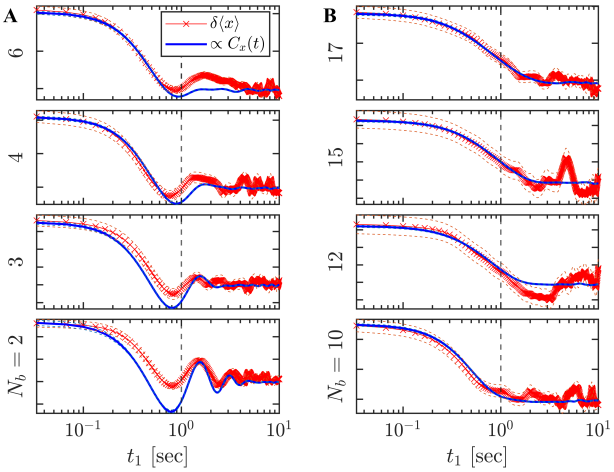

FIG. 11. **FDR results with different numbers of bbots. A,B.** Generalized FDRs with $T_{\mathrm{eff}} \sim \langle \Delta x^2 \rangle_0$ for $N_b = \{2, 3, 4, 6, 10, 12, 15, 17\}$ bbot baths. The results were obtained for an ensemble average of $M = 375$ perturbation sequences, with the same tracer $m \approx 1$ g, gravitational stiffness $k \approx 28.2\ \mathrm{g/s}^{-2}$, and fan operating voltage with $\Delta x(V) < \sigma_x$. The vertical dashed lines are $T_c = 1$ s.

[1] O. Dauchot and V. Démery, Dynamics of a self-propelled particle in a harmonic trap, Phys. Rev. Lett. **122**, 068002 (2019).

[2] M. Heckel, A. Glielmo, N. Gunkelmann, and T. Pöschel, Can we obtain the coefficient of restitution from the sound of a bouncing ball?, Phys. Rev. E **93**, 032901 (2016).